Increase in Surface Friction Dominates the Observed Surface Wind Speed Decline during 1973–2014 in the Northern Hemisphere Lands

ZHENGTAI ZHANG AND KAICUN WANG

State Key Laboratory of Earth Surface Processes and Resource Ecology, College of Global Change and Earth System Science, Beijing Normal University, Beijing, China

DELIANG CHEN

Regional Climate Group, Department of Earth Sciences, University of Gothenburg, Gothenburg, Sweden

JIANPING LI

College of Global Change and Earth System Science, Beijing Normal University, Beijing, China

ROBERT DICKINSON

Department of Geological Sciences, Jackson School of Geosciences, The University of Texas at Austin, Austin, Texas

(Manuscript received 15 October 2018, in final form 23 July 2019)

ABSTRACT

During 1973–2014, a reduction trend in the observed surface wind speed (10 m) in the Northern Hemisphere lands has been widely reported; this reduction is referred to as ''global stilling.'' The primary determining factors of global stilling include atmospheric circulation, turbulent friction, and surface friction when ignoring the vertical influencing factors. Most of the existing studies on the attribution of global stilling do not take changing surface friction into account. In addition, there are other changes in the climate system, such as aerosol loading, which could have an impact on atmospheric circulation, but are not included in the majority of current models either. Here, we developed a novel approach based on modeled winds calculated from sea level pressure observations and applied the method to approximately 4000 weather stations in the Northern Hemisphere lands from 1973 to 2014 to attribute the stilling in the three factors. In our methods, we neglected the vertical influencing factors on surface wind speed but took the aerosols' changes on atmospheric circulation and gradual urbanization effect on surface wind speed into account. We found that atmospheric circulation has dictated the monthly variation in surface wind speed during the past four decades. However, the increased surface friction dominates the long-term declining trend of wind stilling. Our studies had uncertainties while neglecting the influence of vertical factors on surface wind stilling, despite most of the existing studies showing their effect was minor compared to the three factors explored in our study.

1. Introduction

Many studies have shown that the observed surface wind speed (OWS) has substantially reduced in China (Fu et al. 2011; Guo et al. 2011; Lin et al. 2013; M. Xu et al. 2006), Canada (Wan et al. 2010), the United States (Pryor et al. 2009), Australia (McVicar et al. 2008; Troccoli et al. 2012), and Europe (Achberger et al. 2006; Dumitrescu et al. 2015; Earl et al. 2013; Azorin-Molina et al. 2016); this reduction is known as the ''global stilling'' phenomenon (Roderick et al. 2007; Wu et al. 2018a; Hartfield et al. 2018).

Previous studies have explored global stilling from atmospheric circulation and surface roughness change perspectives through model simulations/reanalysis data (Vautard et al. 2010). There are a few studies that take surface friction changes into account. One such example (Jacobson and Ten Hoeve 2012) shows that global urbanization (all infrastructure worldwide) could cause a slight decrease in OWS, based on 20-yr transient climate model simulations. However, most of

Denotes content that is immediately available upon publication as open access.

Corresponding author: Kaicun Wang, kcwang@bnu.edu.cn

DOI: 10.1175/JCLI-D-18-0691.1

the existing climate models do not include the impact of changing surface friction caused by processes such as gradual urbanization. Although reanalysis data are widely used in climate change research (Brönnimann et al. 2018; Kalnay and Cai 2003; Wang et al. 2015; L. M. Zhou et al. 2004; C. Zhou et al. 2017), these data only include monthly climatology of aerosols and do not allow aerosols to change annually (Wang et al. 2015). Thus they cannot reflect the effect of increasing atmospheric aerosol loading on atmospheric circulation (Jacobson and Kaufman 2006; Jacobson 2014; Wang et al. 2009). Because the surface wind speed is impacted by various atmospheric circulations, studies using an atmospheric circulation index (Azorin-Molina et al. 2014) to study the effects of stilling are only suitable at the local scale.

Wind is generated by pressure gradients and modified by friction and the Coriolis force due to Earth's rotation (Markowski and Richardson 2010). The frictional force can be separated into a surface friction force (due to the damping effect of surface roughness) and the turbulent friction force (due to turbulent dissipation within the boundary layer) (Wu et al. 2018a). Surface friction always reduces the OWS, while turbulent friction redistributes momentum to reduce the wind speed gradient among different levels. Surface wind speed usually increases with height. At the same time, turbulent friction, which relates to atmospheric stability, brings more momentum from higher levels to lower levels, reduces high-level winds, and increases low-level winds.

Frictional forces have important roles on OWS variations; however, there have been no quantitative analysis of two types of friction forces that influence OWS in the Northern Hemisphere lands to our knowledge. Here, we developed a novel approach based on modeled wind speed (MWS) calculated from sea level pressure (SLP) observations, which permits us first to calculate MWS at approximately 4000 weather stations in the Northern Hemisphere from 1973 to 2014 to attribute the stilling. Observations (Li et al. 2011) and theoretical analysis (Fan et al. 2005) show that surface friction force has a stronger influence on strong winds than that on weak winds when air flows across a similar underlying surface, and surface friction force is the product of a friction coefficient (determined by the surface roughness) and OWS.

In our study, we focused on the effect of surface friction force on the OWS caused by a surface roughness change, so we introduced a constant friction coefficient when calculating the MWS (Wu et al. 2016). In this way, surface friction force differences between OWS and MWS are determined by friction coefficient differences (i.e., surface roughness changes) only. Because the friction coefficient is set constant, observed SLP is the only input variable in calculating MWS besides the Coriolis factor, which depends on latitude. MWS is supposed to reflect the changes of atmospheric circulation. Since SLP is also influenced by anthropogenic activities such as greenhouse gases and aerosols emissions (Gillett et al. 2003), the use of observed SLP included the aerosols' effect on atmospheric circulation. The MWS is the wind speed under the balance among the pressure gradient force, Coriolis force, and surface friction. The difference between the OWS and MWS reflect the influence of turbulent friction force and surface friction force caused by surface roughness changes on the OWS, which makes it possible to evaluate contributions of atmospheric circulation and friction forces to OWS decline in the Northern Hemisphere lands.

2. Datasets

The daily surface wind speed in China was collected at 2419 meteorological stations from 1973 to 2014 by the China Meteorological Administration (CMA), and the wind speed data were recorded at a standard height of 10 m. The data via the CMA were strictly quality controlled, including checks for climatological, station, and regional outliers and for internal, temporal, and spatial consistencies. In areas outside of China, we used daily data recorded from Global Surface Summary of the Day (GSOD) distributed by the National Climatic Data Center (NCDC), and the data underwent an extensive automated quality control by the Air Weather Service.

Data from more than 9000 stations are typically available across the world, and most stations' records began in 1973. In the trend analysis, we selected approximately 4000 stations in Northern Hemisphere lands according to the following criteria: 1) less than 20% missing data and 2) correlation coefficients between MWS and OWS that passed the t test at the 95% significance level. To eliminate statistical errors on regional studies caused by uneven distribution of stations, we divided all the stations into $3° \times 3°$ grids first, and then used the area-weighted averaging method for statistical analysis (Zhou and Wang 2017).

Similar to the surface wind speed, the daily surface pressure data in China were from 2419 stations of the CMA, and other areas outside of China were from the GSOD stations. Since many GSOD surface pressure data were missing; we added surface pressure data from the Integrated Surface Pressure Databank (ISPD), version 2 (v2), data released by the University Corporation for Atmospheric Research (UCAR) and the National Center for Atmospheric Research (NCAR) at the same sites to increase the consistency of the data. The ISPD contains the largest collection of pressure

observations at weather stations in the world (Cram et al. 2015).

Furthermore, the homogeneity of the surface pressure data is very important for our subsequent calculation of the MWS. Therefore, we used the penalized maximal *f* (PMF) test of the RHtestV4 package to homogenize the daily surface pressure first (Wang 2008). Then we converted the surface pressure of the studied station into the SLP to calculate the MWS. There can be large errors when converting the surface air pressure into SLP for high-altitude stations, thus we removed these station with help of the *t* test mentioned above. That way we only included relatively low-altitude regions to reduce errors caused by surface pressure converted to SLP as far as possible.

In this study, we estimated the two types of frictions by subdividing the OWS and MWS into sunny and cloudy days following the method proposed by Wu et al. (2018a). The determination of sunny and cloudy days was mainly based on the amount of clouds. If the cloud cover was greater than 80% on a given day, it was considered cloudy, and if the cloud cover was less than 20%, it was considered sunny. The cloud data in China derive from the CMA, while those from outside of China are from Integrated Surface Data Lite (ISD-Lite), which records hourly data that were converted into daily averages.

To examine relationship between OWS and land greening, we used leaf area index (LAI) from the Global Land Surface Satellite (GLASS) dataset. The GLASS data were derived from the AVHRR, MODIS, and Carbon Cycle and Change in Land Observational Products from an Ensemble of Satellites (CYCLOPES) reflectance and LAI products using general regression neural networks (Xiao et al. 2014). The GLASS LAI provides global LAI data at 8-day temporal resolution and 1- or 5-km spatial resolution from 1982 to the present, and has been demonstrated to have high credibility in reflecting global LAI changes (Jiang et al. 2017; Xiao et al. 2016). We used the 5-km dataset from 1982 to 2014. For each of the stations chosen, the LAI in the growing season (April–October) from the nearest grid cell is assigned.

3. Methodology

a. Calculating the MWS

According to dynamic meteorology, the surface wind speed is calculated as follows:

$$-\frac{\nabla p}{\rho} + F + f = 0, \tag{1}$$

$$f = f_t + f_s, \tag{2}$$

$$f_s = kV, \tag{3}$$

where ∇p denotes pressure gradient, ρ represents density of air, F represents the Coriolis force, f represents frictional force consisting of f_t (turbulent friction force) and f_s (surface friction force), k represents the friction coefficient, and V represents the surface wind speed. The MWS is the wind speed under the balance of the pressure gradient force, Coriolis force, and surface friction force,

$$-\frac{\nabla p}{\rho} + F + f_s. \tag{4}$$

In the calculation, we regarded p as a function of location,

$$p = ax + by + c, \tag{5}$$

where x and y are longitudes and latitudes of locations, respectively; a and b are pressure gradient in longitudinal and latitudinal directions, respectively; c is the constant term. Therefore, we need the air pressure values from at least three stations around the studied stations to derive the MWS. More details about the calculation of the pressure gradient force can be seen in previous studies (Wu et al. 2016; Wang et al. 2009).

A pressure triangle based on the distribution of the stations is needed to calculate the pressure gradient force (Wan et al. 2010; Minola et al. 2016; Wang et al. 2009). If any one of the three stations has large errors in the observed SLP, large errors in estimated pressure gradient and associated wind will occur. If any of these three stations have a missing data on a certain day, no MWS can be estimated on that day. More importantly, this method is only reliable under the condition of a steady flow field.

To ensure a reasonable accuracy of the pressure gradient estimation, we selected the stations within 3° for each studied station. This is justified by the fact the horizontal range of cold fronts usually extends from 80 to 300 km (Carlson 1991). The local SLP changes with the invasion of the air mass; therefore, stations within 3° show changes in the air pressure system, which are presented in the calculated MWS. At the same time, we used observed SLP and constant friction coefficient in calculating MWS, the surface friction differences in OWS, and MWS reflect surface roughness changes caused by actual friction coefficient and constant friction coefficient differences, which reflect gradual urbanization around studied stations, while this could not be accomplished via model simulations or reanalysis data.

To ensure accuracy of our estimates, we required that there were at least 10 stations around the studied station, otherwise, the station was discarded.

Second, we chose the stations selected at the first step by taking the studied station as the center to build pressure triangles, which can make up many pressure triangles. To reduce the number of calculations, if the combinations of these surrounding stations exceed 1000, we chose 1000 combinations randomly to calculate the MWS. Otherwise, we chose the combinations of all stations.

Finally, we chose the values of the 10th percentiles of these values as the MWS of the studied station (we detected 50th percentiles every 5th quartile from the 5th percentiles, and the reason for selecting 10th percentiles will be presented in the next section). In our new method, we set up air pressure tracking triangles. In this way we cannot only eliminate the shortage of SLP data at the individual stations or the shortcomings in the large errors of the SLP data, but also build pressure triangles properly according to the weather system, by not only using fixed pressure triangles to calculate the pressure gradient. Thus, our approach can be applied to a global scale well.

b. *Verifying MWS*

Accurate and reasonable MWS is very important for our research, therefore, we evaluated the MWS as follows. We first focused our research on 2419 stations in China. In section 3a, we mentioned that the selection of the 10th percentiles from approximately 1000 studied station combinations as the studied station's MWS. Here, we show why choosing the 10th percentiles is the best choice.

Figure 1 is a schematic diagram of two simple flow fields. The actual pressure fields are very complicated. However, in the idealized calculation, we can hypothesize that the flow field is simply divided into a constant field and a changing field at the regional scale. If the station we studied is in a constant pressure flow field, then formula 5 is established. That is, the pressure is a linear function of location regardless of using fixed stations or arbitrarily choosing station combinations (Figs. 1a,c), they all meet the above relationship (similar to the examples shown with black triangles in Fig. 1a and the black, pink, and green triangles in Fig. 1c). If there are no errors in the observed surface pressure, it is accurate to take the studied station as the center and use fixed or surrounding station combinations to calculate the MWS.

In reality, pressure field changes, and the change in the pressure field are associated with various weather phenomena. Thus, a few days later, the pressure field at the studied station may be turned into that in Fig. 1b. As

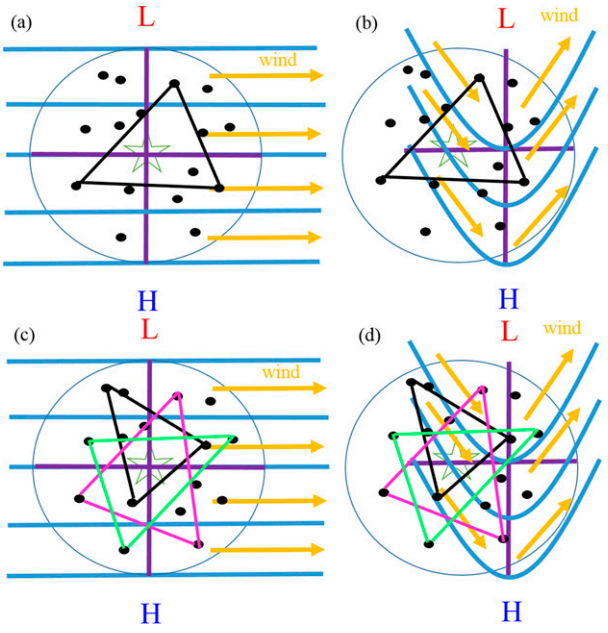

FIG. 1. Schematic diagram of the pressure gradient force calculation in two typical flow fields between the (a),(b) previous study and (c),(d) new method. (a) Previous calculation method in the constant flow field. (b) Previous calculation method in the changing flow field. (c),(d) As in (a) and (b), but for the improved method in this study. The light blue line represents isobars, the red "L" represents the low pressure center, the blue "H" represents the high pressure center, the yellow arrow represents the direction of the wind, the pentagram represents the studied station, the circle represents the distance within 3° around the studied station, and the black dots represent the surrounding stations. The black lines in (a) and (b) represent the use of fixed triangles around the studied stations to calculate the pressure gradient force. The black, pink, and green lines in (c) and (d) show a simple example of the three different combinations of triangles used in this study.

shown in Fig. 1b, a turning point can be seen in the change in the air pressure field. In this case, the linear relationship between the pressure field and the location can be divided into two general segments, which are represented by the vertical purple line on the left and right sides. In this case, it is problematic to use the three fixed stations in Fig. 1b or choose a combination of three stations around the studied station at random, as shown in Fig. 1d. The pressure field and location satisfy a linear equation to the left of the vertical purple line, while the other linear equation is satisfied to the right. In this case, only the combinations of stations to the left of the vertical purple line (black and pink triangles in Fig. 1d) meet the linear relationship between the pressure field and location of the studied station. Therefore, in the changing field, the use of fixed triangles or all surrounding station combinations is not applied to calculate the MWS.

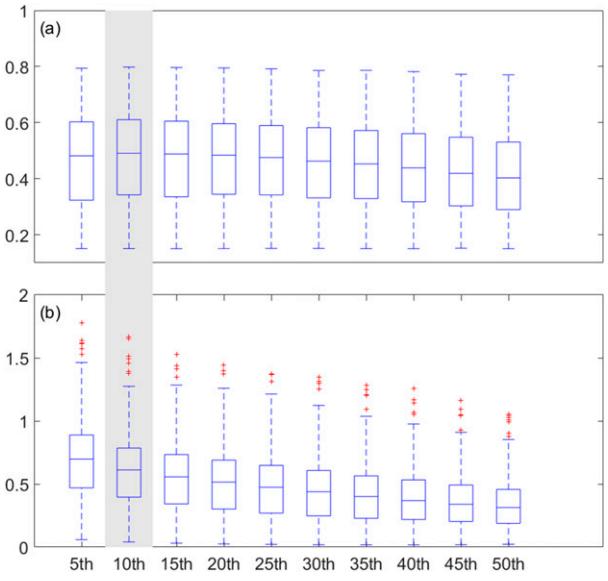

FIG. 2. The results of the MWS using the 5th–50th percentiles of the surrounding studied station combinations within 3°. (a) Correlation coefficient between the OWS and MWS calculated by their corresponding percentiles in China. (b) Coefficient of the variation ratio between the MWS and OWS in China. The gray shaded area indicates the final percentile selected.

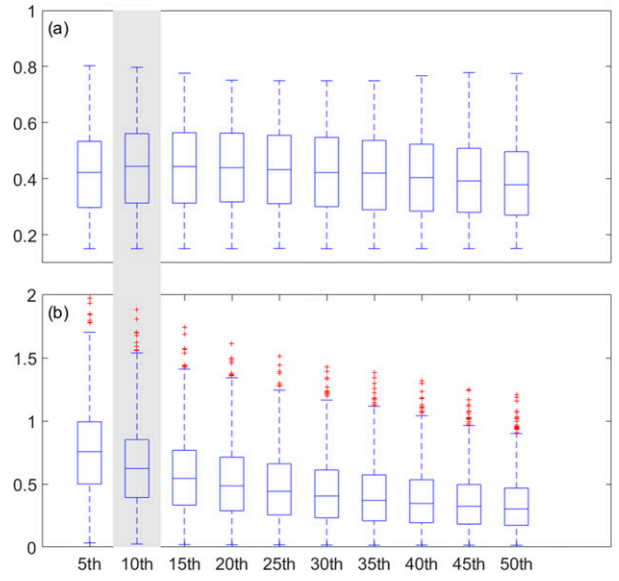

FIG. 3. As in Fig. 2, but for the surrounding studied station combinations within 1°–3°.

If one uses a fixed triangle around the studied station and does not take pressure fields changes into account, the situation is unrealistic. Therefore, we proposed an improved method that uses percentiles of the studied station combinations, and we determined 5th–50th percentiles of approximately 1000 triangle combinations. Figure 2 shows the results of the MWS using the 5th–50th percentiles. The correlation coefficients between MWS and OWS was calculated by their daily time series annually from 1973 to 2014 and the median of correlation coefficients of the 42-yr coefficient coefficients was reported here, which demonstrated the capability of the MWS in reflecting daily variability of surface wind speed.

From Fig. 2a, we can see that the correlation coefficients for small percentiles are higher than those for the higher percentiles. Figure 2b shows that the MWS coefficient of variation is lower than that of the OWS, which shows that the MWS is relatively stable, which is easy to understand. The modeled winds describe the steady flow of air, while the surface winds are subject to impact of surface roughness changes. There are no large differences among the small percentiles. However, the MWS should be higher than the surface wind speed as a whole. Using the 5th percentiles at some stations results in an MWS that is less than the OWS. Therefore, we finally adopted the 10th percentiles of these calculated values for the combinations as the studied station MWS.

To validate the stability of the new method, we calculated the MWS by using station combinations within 1°–3° around the studied station. In this way, the derived modeled wind can be considered free of the influence of small-scale weather systems due to the choice of the distances among the stations used for calculating MWS. The results shown in Fig. 3 are similar to those in Fig. 2 because the method of using percentiles of the surrounding studied station combinations within 3° is similar to the Monte Carlo simulation, and the calculated MWS is steady because the influence of small-scale weather systems should have been filtered out. In what follows, the MWS using station combinations within 3° around the studied station was calculated directly.

The correlation coefficients between the MWS and OWS are shown in Fig. 4. The correlation coefficients between the MWS and OWS reached 0.7–0.8 and was higher in the plain areas but decreased at high altitudes and over complex terrains. This is because the OWS variations over complex terrains more complicated than MWS and we will discuss in section 5.

c. *Separating friction force into surface and turbulent friction force*

Because the friction coefficient was set to be constant when calculating the MWS, the impact of friction force on the OWS can be obtained by OWS-MWS. To divide the friction force into a surface friction force and turbulent friction force, we follow the method of a previous study (Wu et al. 2018b). It was assumed that sunny days are conducive to convection compared to cloudy days. The turbulence friction on sunny days includes both thermal

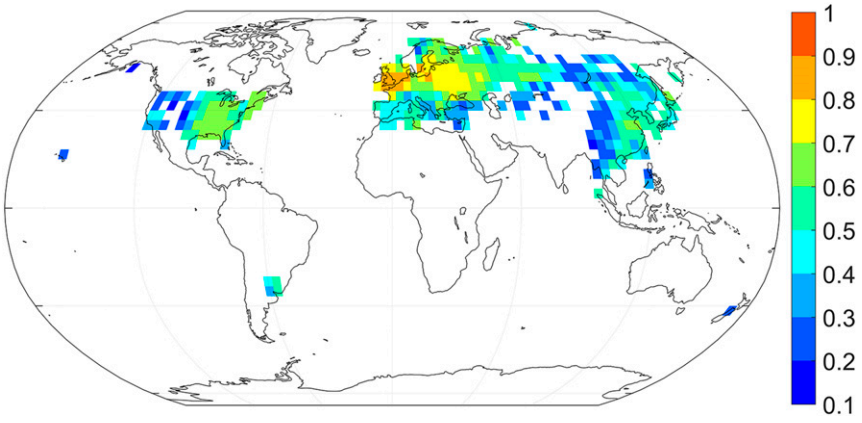

FIG. 4. The distribution of the annual median correlation coefficients between the MWS and OWS. We calculate the annual MWS and OWS correlation coefficients from 1973 to 2014 and then draw the distribution of the median correlation coefficients of the 42-yr dataset for each station.

and mechanical turbulence, while it mainly includes mechanical turbulence induced by the vertical shear of the horizontal wind at different heights on overcast days. Actually, the OWS differences between overcast days and sunny days are about 0.2–0.3 m s^{-1}. If we neglect the weak mechanical turbulent mixing differences between two types of days, the difference between the OWS on sunny and overcast days reflect the combined effect of pressure gradient force and turbulent friction force.

The MWS reflects the change in surface-level pressure; therefore, the difference in the MWS between sunny days and cloudy days (ΔMWS) reflects the pressure gradient force differences in the MWS between the two weather conditions. At the same time, the surface friction can generally be regarded as the same given that the OWS difference under the two weather conditions can be ignored. Therefore, the differences between the OWS on sunny and overcast days (ΔOWS) include not only the difference in the pressure gradient force, but also the effect of turbulent friction. Therefore, the influence of turbulent friction on the OWS can be obtained by ΔOWS −ΔMWS, and the surface friction force caused by surface roughness change on the OWS can be obtained by (OWS − MWS) − (ΔOWS − ΔMWS). In this way we isolated the influences of the two types of frictional force on the OWS.

4. Results

a. *Surface wind speed variations in the Northern Hemisphere lands*

Figure 5 shows the trends of the OWS and MWS from 1973 to 2014. The OWS showed a substantial reduction in most parts of the Northern Hemisphere (Fig. 5a), with a significant decreasing trend of −0.3 to −0.2 m s^{-1} decade^{-1}. However, the MWS did not show a significant decreasing trend. In fact, it increased slightly in Europe and a small part of eastern Asia. The reanalysis data such as NCEP–NCAR did not show a significant trend in the Northern Hemisphere between 1979 and 2008 either (Vautard et al. 2010). Because the existing reanalysis ignores the impact of surface roughness changes due to their lack of interannual variability in land cover and land use, the reanalysis reflects most of the changes in the OWS as a result of atmospheric circulation variability. The MWS is a result of the pressure field, which directly describes surface wind speed variations under the influence of atmospheric circulation. Therefore, the near-zero trend of the MWS in Fig. 5 can be taken as confirmation for the results based on the reanalysis data. However, it should be noted that reanalysis data have deficiencies in describing of other changing conditions in the atmosphere, such as atmospheric aerosol loading, which may lead to a trend in the surface wind speed in the reanalysis that is slightly different from that in the MWS.

b. *Frictional influence on surface wind speed*

To show regional differences in friction, we divided the studied stations into three areas: North America (25°–50°N, 95°–60°W), Europe (35°–70°N, 15°W–40°E), and eastern Asia (20°–48°N, 110°–150°E). The influence of surface friction on the OWS increased in east Asia, most of Europe and North America during 1973–2014 (Fig. 6a). However, the increasing trends in the last two areas are much lower than that in east Asia. The impact of turbulent friction on the OWS decreased in the Northern Hemisphere excluding a small part of North America (Fig. 6b).

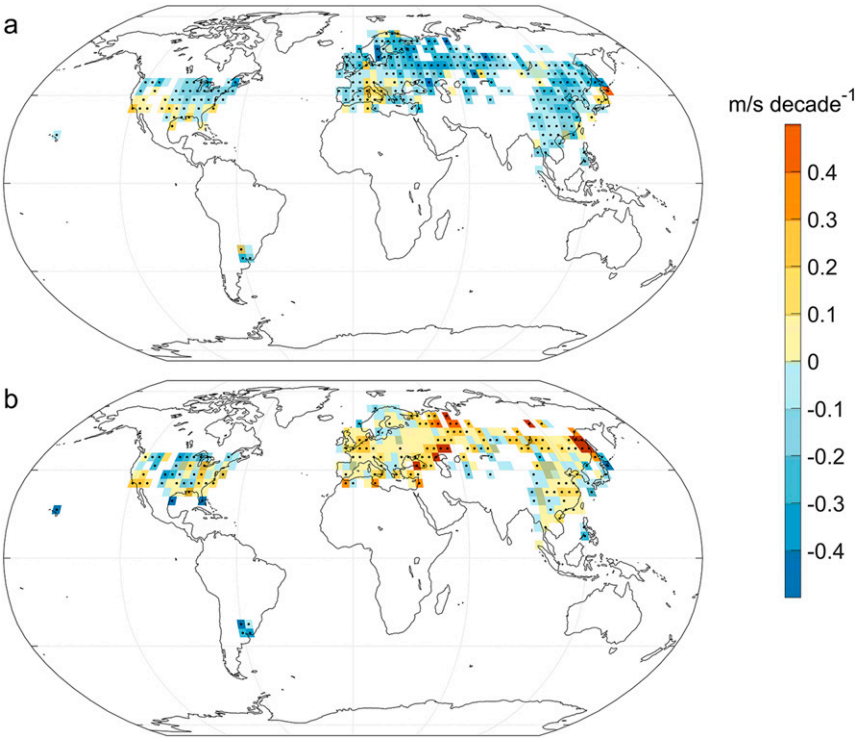

FIG. 5. (a) Observed surface wind and (b) modeled wind trend distributions from 1973 to 2014 in the Northern Hemisphere. Regions with black dots in (a) and (b) indicate that these areas passed the significance test at the 0.05 level based on the Mann–Kendall test.

Regarding linear trends in the OWS as a function of the linear trends of the two types of friction influences on the OWS, the surface friction has a close linear relationship with the trend in OWS (Fig. 7a). The decrease in OWS is associated with surface friction increases because surface friction always has a damping effect on the OWS. Compared to surface friction, the influence of turbulent friction on the OWS is more complex and related to momentum exchange within the planetary boundary layer. Therefore, it does not have a linear relationship with the OWS change (Fig. 7b).

The annual time series of the two types of frictional force effects on the OWS in the three regions are shown in Fig. 8. The surface friction force shows a decreasing trend in all three regions (Fig. 8a): the impacts of the surface friction force on OWS in eastern Asian, North America and Europe are -0.19, -0.13, and $-0.07\,\mathrm{m\,s^{-1}}$ decade^{-1}, respectively.

Figure 9 shows the annual time series of the OWS and MWS, which shows that the difference between the OWS and MWS has become increasingly obvious since the 1990s (Fig. 9c). Satellite observations have indicated significant land greening in the northern extratropical latitudes since the early 1980s (Mao et al. 2016; Myneni et al. 1997; Zhu et al. 2016), which might be one of the reasons for the increase in surface friction force and decrease in OWS over the Northern Hemisphere lands. The effect of turbulent friction on the OWS shows a slight increasing trend in Europe and eastern Asia, but it does not show an obvious trend in North America (Fig. 8b).

To quantify relationship between land greening and OWS reduction, we examined the relationship between global long-term satellite LAI records in growing season (from April to October) with OWS (also in growing seasons). Figure 10 shows the OWS trends and their relationship with LAI trends. It was found that 83% of stations witnessed a positive LAI trend in growing seasons, the LAI trend in North America, Europe, and eastern Asia are 0.04, 0.06, and $0.03\,\mathrm{m^2\,m^{-2}}$ decade^{-1}, respectively. Also, there is a significant negative correlation between the increasing trend of LAI and the decreasing trend of OWS, and the regression line for the median OWS trend versus LAI trend is $y = -0.26 - 0.33x$ (coefficient of determination $R^2 = 0.41$, Fig. 10b), which supports the view that land greening reduce surface winds. However, a quantitative relationship between LAI and surface roughness is difficult to establish.

It is worth mentioning that unlike temperature or other meteorological variables, OWS are more sensitive

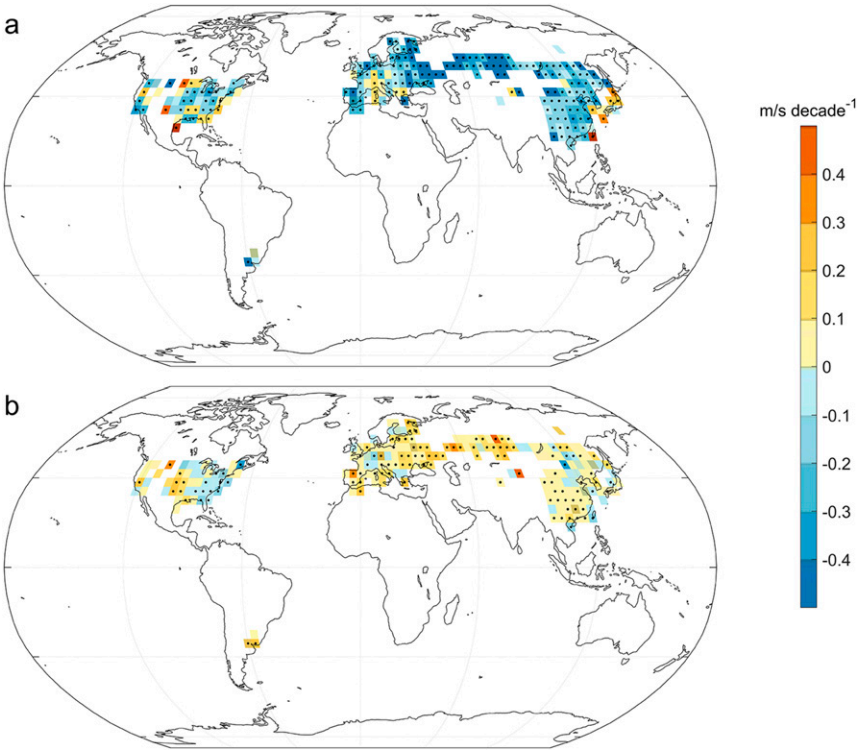

FIG. 6. Trends in (a) surface friction and (b) turbulent friction influences on the OWS between 1973 and 2014 in the Northern Hemisphere. Regions with black dots in (a) and (b) indicate that these areas passed the significance test at the 0.05 level based on the Mann–Kendall test.

to environment changes around the studied stations (Han et al. 2016; Si et al. 2018; Wan et al. 2010). The environment close to the stations could attribute 70% changes of the OWS (Wever 2012). Local roughness, with a typical length scale up to approximately 500 m, attributed 35% and the mesoscale roughness up to 8 km contributed another 35%. This is the main reason why wind speeds are negative correlated with vegetation indices generally (Vautard et al. 2010). However, it should be pointed out that there are studies showing that wind speeds are not correlated with vegetation indices at all (McVicar et al. 2012).

Some land-cover types around studied stations do not dominate the average vegetation indices in grid scale (5 km), but they could play important roles in the studied stations' OWS. From our study, there is a link between LAI trend and OWS decline over Northern Hemisphere lands in general. The meteorological variables used in our MWS, such as sea level pressure, wind speed, and friction coefficient, include the effects of both large-scale and local factors, which is the advantage of our study compared to most of the previous studies.

OWS changes are caused by both large-scale and local factors (Wu et al. 2016). Apart from land greening, urbanization is also one of the main factors that are closely correlated with surface roughness (McVicar et al. 2012; Wever 2012; Wong and Nichol 2012). Thus, it was considered another main reason causing OWS decline in the last four decades. In this period, eastern Asia (especially China) experienced rapid urbanization, which also caused an increase in surface roughness around the weather stations (Grimm et al. 2008; Jones et al. 2008; Ren et al. 2008; Sun et al. 2016). Therefore, the effect of surface friction on the reduction in OWS becomes increasingly obvious. At this stage, North America and Europe had already finished rapid urbanization before the study period; therefore, their levels of urbanization were much slower than those of eastern Asia (Grimm et al. 2008). As a result, the decrease in the OWS due to surface friction in these two areas is not as strong as that in eastern Asia.

There is a simple theory developed to link roughness height and roughness in sparse roughness elements areas, the roughness height should scale as $z \sim h\lambda^{1.33}$ (Raupach 1994; Raupach 1992), where z is roughness height, h and λ are the height and frontal area index of the roughness elements, respectively. By using sensitivity simulations with the MM5 model, Vautard et al. (2010) found that a doubling of surface roughness height would lead to a decrease of OWS by 0.26–0.33 m s^{-1},

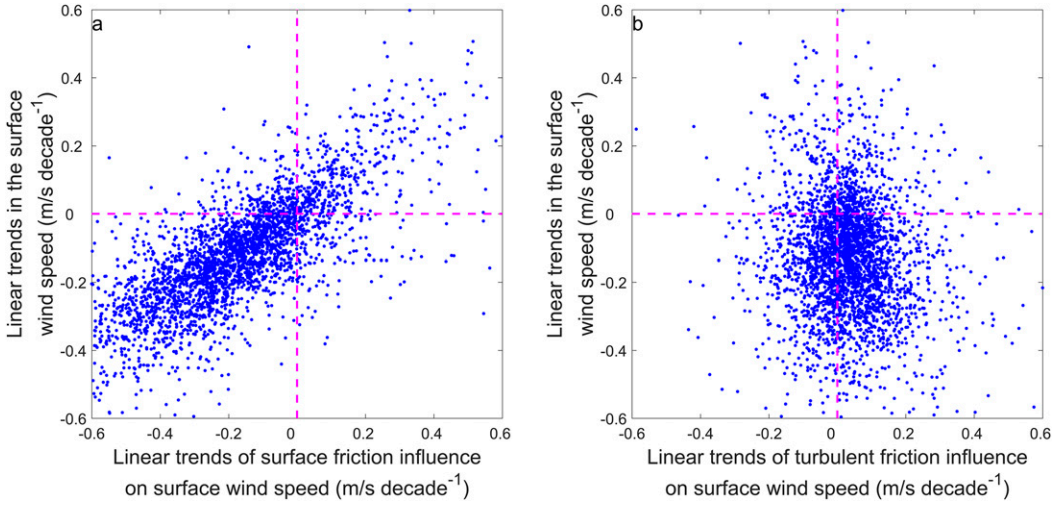

FIG. 7. Scatterplots of the linear trends in the OWS ($m\,s^{-1}$ $decade^{-1}$) as a function of the linear trends of the two types of friction influences on the OWS ($m\,s^{-1}$ $decade^{-1}$). (a) Linear trends between the OWS and surface friction influence on the OWS. (b) As in (a), but for the turbulent friction influence on the OWS.

which is in the range of observed wind decreases in our studied periods. Wever (2012) found that the surface roughness increase in the Netherlands could have doubled during the period of 1962–2009. Our studied period is from 1973 to 2014, which is the period during which all over the Northern Hemisphere lands underwent significant urbanization and land greening (Grimm et al. 2008; Mao et al. 2016).

c. *Attribution of the reduced surface wind speed*

We applied a multivariate regression analysis that is commonly used in meteorology (Du et al. 2017; Schlatter et al. 1976; C.-Y. Xu et al. 2006) to quantitatively analyze the contribution of atmospheric circulation to the OWS decline, and the relative roles played by the two types of friction. In regression analysis, we used monthly anomalies to remove seasonal cycles first. We found differences in the monthly variation in the OWS caused by atmospheric circulation in the three regions: its contributions in North America, Europe, and eastern Asia were 41%, 71%, and 50%, respectively (Fig. 11a). The monthly variation in the OWS in Europe is mainly due to the effect of atmospheric circulation, but its impact is less in eastern Asia and North America. In contrast, the

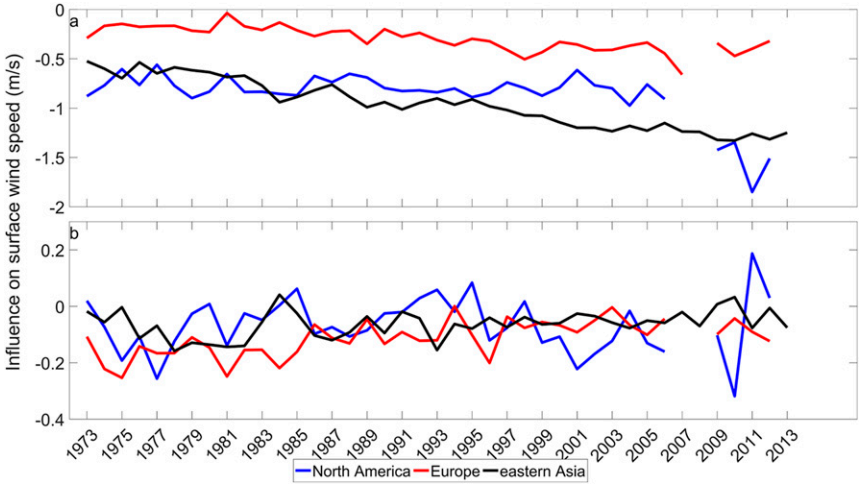

FIG. 8. Time series of annual influences on the OWS caused by (a) surface friction and (b) turbulent friction. The blue, red, and black lines represent North America, Europe, and eastern Asia, respectively.

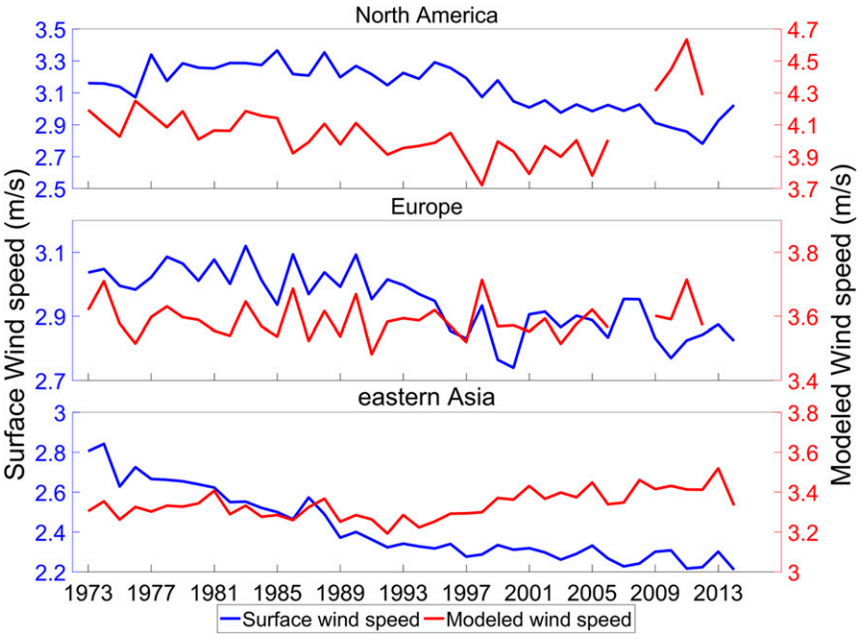

FIG. 9. Annual time series of the MWS and OWS speed in different regions. The blue lines represent the OWS, and the red lines represent the MWS.

contribution of atmospheric circulation to the annual variation in the OWS shows a large difference; its contributions in North America, Europe, and eastern Asia are 2%, 15%, and 48%, respectively (Fig. 11b), which indicates that atmospheric circulation explains little of the annual variations in the surface wind speed except for those in eastern Asia.

We used MWS calculated from SLP to present atmospheric circulation, because SLP could also be influenced by anthropogenic activities such as greenhouse gases and aerosols emissions (Gillett et al. 2003), the greenhouse gases and aerosols emissions are the most obvious in eastern Asia, so we think this might be the main reason why the atmospheric circulation has a relatively large annual variance contribution in eastern Asia compared to North America and Europe.

The contributions of the three factors to the OWS depend on both their variabilities and trends. The proposed method includes the contributions of both. We found that the contributions of atmospheric circulation to the OWS reduction in North America, Europe, and eastern Asia were 21%, 1%, and −7%, respectively (Fig. 11c), which are much less than the contributions to the monthly variations. Evidently, atmospheric circulation was the main cause of OWS seasonal variability in the Northern Hemisphere, but not the trend in the OWS. In contrast, surface friction is the main cause of global stilling, but plays a minor role in the monthly variation in the OWS. The contributions of surface friction to the decline in the OWS in North America, Europe, and eastern Asia are 81%, 125%, and 133%, respectively. The latter two trend contributions are greater than 100%, because the trend contributions of turbulent friction on the OWS decline is negative (Fig. 11c), which means the turbulent friction influence on wind speed are becoming weaker.

d. *Uncertainty analysis*

We studied OWS changes from the two-dimensional equation of atmospheric horizontal motions. However, actual atmospheric motion is a three-dimensional process. With the increase of aerosol emissions in recent years, the aerosols influence on OWS has also attracted more and more attention. Atmospheric aerosols can scatter and absorb solar radiation, resulting in a reduction of surface incident solar radiation and heating of atmospheric boundary layer. This enhances atmospheric stability and reduce vertical transport of horizontal momentum, which could reduce OWS (Jacobson and Kaufman 2006).

From the viewpoint of 3D motion, Zeng et al. (2018) decompose the influencing factors for OWS into advection, pressure gradient force, convection, and frictional force, respectively. They find that advection is two to three orders of magnitude less than the magnitudes of the other three factors, so that the effect of advection on OWS is very weak and can be negligible. The magnitudes of other three factors are of the same order, the pressure

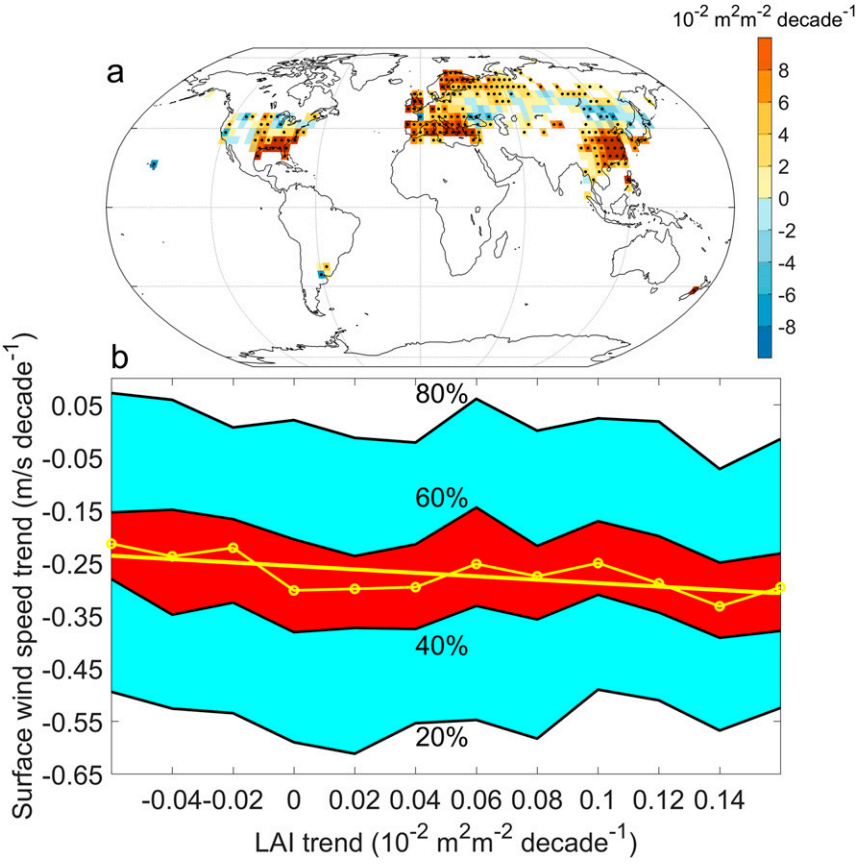

FIG. 10. Surface wind trends and their relationship with LAI trends. (a) Surface wind stations' LAI trends in growing season (April–October). (b) Surface wind trends over the stations of each percentile of the LAI trend distribution, together with the corresponding wind trend distribution (20%–40% and 60%–80% in aqua, 40%–60% in red), vs each percentile of LAI trends. The regression line for the median surface wind trend ($y = -0.26 - 0.33x$, $R^2 = 0.41$) is shown in yellow.

gradient force and frictional force effect have nearly the same value, but the convection is are usually 3–5 times lower than pressure gradient force. Further, the convection has an 8%–13% contribution to the OWS variations.

Through investigating OWS over China using satellite data and numerical studies over the south coast air basin in California, Jacobson and Kaufman (2006) proposed that aerosol particle and precursor gases may reduce OWS by up to 8% locally. There were numerical studies also showed that the aerosol emissions could induce $0.03\,m\,s^{-1}$ OWS decline during 1976–2005 over the Northern Hemisphere lands, while the OWS decline in the same period was $0.33\,m\,s^{-1}$, that was nearly 10% trend contribution (Bichet et al. 2012). For China, the aerosols-induced OWS decline was $-0.025\,m\,s^{-1}$, and the OWS decline was $-0.54\,m\,s^{-1}$; the aerosols' trend contribution was even less than 10%, which was also consistent with study conducted by Jacobson and Kaufman (2006).

Overall, the convection effect on OWS was minor compared to pressure gradient force and frictional force effect. Therefore, the effect of vertical transport of horizontal momentum on OWS was neglected. We discussed the influences of two main important factors (pressure gradient force and frictional force) on OWS, and our results about the attribution analysis of OWS decline have an error range about 10%. As the contribution of the surface friction force to the OWS decline is much greater than this error range, we conclude that it is the surface friction dominated OWS decline in the last four decades in the Northern Hemisphere lands.

5. Conclusions and discussion

Based on the observed data during 1973 and 2014, we found that atmospheric circulation played a major role in the monthly variations of OWS in Europe (71%); however, the role of atmospheric circulation in eastern

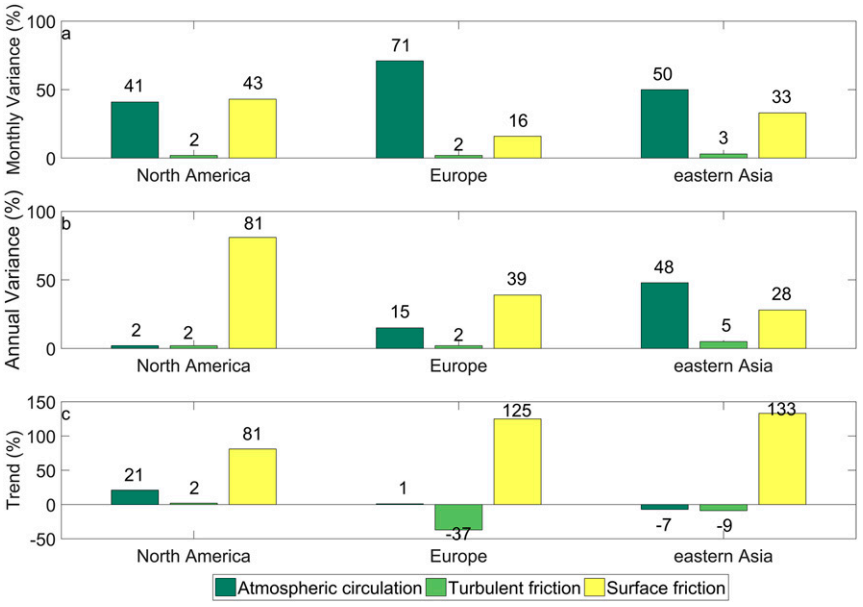

FIG. 11. Analysis of variance and trend contributions of the OWS stilling in the Northern Hemisphere. (a) Monthly variation contribution of changes in the OWS. (b) Annual variance contribution of the OWS change. (c) Trend contribution of the decrease in the OWS. Green, aqua, and yellow represent the contributions of atmospheric circulation, turbulent friction, and surface friction, respectively. For the variance contribution, the analyzed variables were detrended first.

Asia (50%) and North America (41%) was relatively weak. Surface friction is one of the main reasons for the monthly variation in the OWS in North America (43%) and eastern Asia (33%), but its impact on Europe (16%) is relatively low.

Regarding the annual variance, atmospheric circulation contributes little in North America (2%) and Europe (15%) but has a large contribution in eastern Asia (48%). Surface friction dominates the annual variance in the OWS in North America (81%) and Europe (39%). Turbulent friction is not the decisive factor causing the change in the OWS in these three regions. Although surface friction has different contributions to OWS changes in eastern Asia, Europe, and North America, it dominates the OWS decline in all three regions, with contributions of 133%, 125%, and 81%, respectively.

The results presented here are based on observational data that are different from those via the mesoscale model simulation (Vautard et al. 2010), because we studied OWS changes individually from variance and trend perspectives, while the models examined these changes together. Furthermore, we quantified each factor's impact in the corresponding region. Because the vertical influencing factors on OWS decline were neglected in our study, we assessed the uncertainties mainly based on previous studies (Bichet et al. 2012; Jacobson and Kaufman 2006; Zeng et al. 2018). Even though their results showed that aerosols contribution to OWS decline (about 10%) was minor compared to the three factors we explored, there might be large uncertainties in our study, because the uncertainty of aerosols contribution to OWS stilling had large influences on the accuracy of our study. Also, the aerosols emissions were getting more and more serious in the last decade over China, the aerosols contribution to OWS stilling need to be further explored in the future to access the uncertainty of our results.

In addition to the three major factors of atmospheric circulation, turbulent friction, and surface friction, the OWS is also controlled by factors such as topography (Klink 1999), the local turbulence (Nonaka and Xie 2003), and environment (Ozdogan et al. 2006), as well as the performance of anemometers and their changes (Azorin-Molina et al. 2018). The topography does not introduce the interannual variability of the OWS, and the impacts of the other factors are unknown and need further study.

Inhomogeneity of meteorological data caused by weather station relocation has been widely recognized. However, station relocation generally moves the weather station from an urban area to a rural area, which would result in an increase in the OWS in most cases rather than a reduction, as shown by the observed data

(Guo et al. 2011; Li et al. 2011). Figure 9 also shows that there is no obvious increase in the OWS, which implies that the inhomogeneity of the OWS most likely did not significantly affect our results regarding OWS trends at regional scales.

This study quantitatively distinguishes the effect of atmospheric circulations and two types of friction on OWS and contributes to the improved understanding of the wind speed reduction. Surface friction is found to be mostly positively correlated with land-use and land-cover change and urbanizations (McVicar et al. 2012; Wever 2012). Northern Hemisphere lands experienced significant land greening and urbanizations in the last four decades. Thus it was proposed that the surface friction increase might be mainly caused by the combined effects of land greening and urbanization. These two factors were also found to influence the OWS decline by previous studies (Vautard et al. 2010; Wever 2012). However, it was hard to distinguish the effect of greening and that of the urbanizations quantitatively in this study, which needs to be further studied.

Acknowledgments. This work was funded by the National Basic Research Program of China (2017YFA0603601), the National Natural Science Foundation of China (41525018), and the Swedish Research Council (2017-03780). Thanks also go to CMA (http://data.cma.cn/en/?r=data/), NCDC (https://www.ncdc.noaa.gov/), GLASS (http://glass-product.bnu.edu.cn/), and NCAR (https://ncar.ucar.edu/) for providing related data used in our study.

REFERENCES

Achberger, C., D. Chen, and H. Alexandersson, 2006: The surface winds of Sweden during 1999–2000. *Int. J. Climatol.*, **26**, 159–178, https://doi.org/10.1002/joc.1254.

Azorin-Molina, C., and Coauthors, 2014: Homogenization and assessment of observed near-surface wind speed trends over Spain and Portugal, 1961–2011. *J. Climate*, **27**, 3692–3712, https://doi.org/10.1175/JCLI-D-13-00652.1.

——, J.-A. Guijarro, T. R. McVicar, S. M. Vicente-Serrano, D. Chen, S. Jerez, and F. Espírito-Santo, 2016: Trends of daily peak wind gusts in Spain and Portugal, 1961–2014. *J. Geophys. Res. Atmos.*, **121**, 1059–1078, https://doi.org/10.1002/2015JD024485.

——, J. Asin, T. R. McVicar, L. Minola, J. I. Lopez-Moreno, S. M. Vicente-Serrano, and D. Chen, 2018: Evaluating anemometer drift: A statistical approach to correct biases in wind speed measurement. *Atmos. Res.*, **203**, 175–188, https://doi.org/10.1016/j.atmosres.2017.12.010.

Bichet, A., M. Wild, D. Folini, and C. Schär, 2012: Causes for decadal variations of wind speed over land: Sensitivity studies with a global climate model. *Geophys. Res. Lett.*, **39**, L11701, https://doi.org/10.1029/2012GL051685.

Brönnimann, S., and Coauthors, 2018: Observations for reanalyses. *Bull. Amer. Meteor. Soc.*, **99**, 1851–1866, https://doi.org/10.1175/BAMS-D-17-0229.1.

Carlson, T. N., 1991: *Mid-Latitude Weather Systems*. HarperCollins Academic, 507 pp.

Cram, T. A., and Coauthors, 2015: The International Surface Pressure Databank version 2. *Geosci. Data J.*, **2**, 31–46, https://doi.org/10.1002/gdj3.25.

Du, J., K. Wang, J. Wang, and Q. Ma, 2017: Contributions of surface solar radiation and precipitation to the spatiotemporal patterns of surface and air warming in China from 1960 to 2003. *Atmos. Chem. Phys.*, **17**, 4931–4944, https://doi.org/10.5194/acp-17-4931-2017.

Dumitrescu, A., R. Bojariu, M.-V. Birsan, L. Marin, and A. Manea, 2015: Recent climatic changes in Romania from observational data (1961–2013). *Theor. Appl. Climatol.*, **122**, 111–119, https://doi.org/10.1007/s00704-014-1290-0.

Earl, N., S. Dorling, R. Hewston, and R. von Glasow, 2013: 1980–2010 variability in U.K. surface wind climate. *J. Climate*, **26**, 1172–1191, https://doi.org/10.1175/JCLI-D-12-00026.1.

Fan, W., G. Zhiyi, W. Ziku, and L. Hongmin, 2005: Wind speed scaling and the drag coefficient. *Acta Oceanol. Sin.*, **24**, 29–42.

Fu, G., J. Yu, Y. Zhang, S. Hu, R. Ouyang, and W. Liu, 2011: Temporal variation of wind speed in China for 1961–2007. *Theor. Appl. Climatol.*, **104**, 313–324, https://doi.org/10.1007/s00704-010-0348-x.

Gillett, N. P., F. W. Zwiers, A. J. Weaver, and P. A. Stott, 2003: Detection of human influence on sea-level pressure. *Nature*, **422**, 292–294, https://doi.org/10.1038/nature01487.

Grimm, N. B., S. H. Faeth, N. E. Golubiewski, C. L. Redman, J. G. Wu, X. M. Bai, and J. M. Briggs, 2008: Global change and the ecology of cities. *Science*, **319**, 756–760, https://doi.org/10.1126/science.1150195.

Guo, H., M. Xu, and Q. Hu, 2011: Changes in near-surface wind speed in China: 1969–2005. *Int. J. Climatol.*, **31**, 349–358, https://doi.org/10.1002/joc.2091.

Han, S. J., Q. H. Tang, X. Zhang, D. Xu, and L. H. Kou, 2016: Surface wind observations affected by agricultural development over Northwest China. *Environ. Res. Lett.*, **11**, 054014, https://doi.org/10.1088/1748-9326/11/5/054014.

Hartfield, G., J. Blunden, and D. S. Arndt, Eds., 2018: State of the Climate in 2017. *Bull. Amer. Meteor. Soc.*, **99** (8), Si–S310, https://doi.org/10.1175/2018BAMSStateoftheClimate.1.

Jacobson, M. Z., 2014: Effects of biomass burning on climate, accounting for heat and moisture fluxes, black and brown carbon, and cloud absorption effects. *J. Geophys. Res.*, **119**, 8980–9002, https://doi.org/10.1002/2014JD021861.

——, and Y. J. Kaufman, 2006: Wind reduction by aerosol particles. *Geophys. Res. Lett.*, **33**, L24814, https://doi.org/10.1029/2006GL027838.

——, and C. L. Archer, 2012: Saturation wind power potential and its implications for wind energy. *Proc. Natl. Acad. Sci. USA*, **109**, 15 679–15 684, https://doi.org/10.1073/pnas.1208993109.

——, and J. E. Ten Hoeve, 2012: Effects of urban surfaces and white roofs on global and regional climate. *J. Climate*, **25**, 1028–1044, https://doi.org/10.1175/JCLI-D-11-00032.1.

Jiang, C., Y. Ryu, H. Fang, R. Myneni, M. Claverie, and Z. Zhu, 2017: Inconsistencies of interannual variability and trends in long-term satellite leaf area index products. *Global Change Biol.*, **23**, 4133–4146, https://doi.org/10.1111/gcb.13787.

Jones, P. D., D. H. Lister, and Q. Li, 2008: Urbanization effects in large-scale temperature records, with an emphasis on China. *J. Geophys. Res.*, **113**, D16122, https://doi.org/10.1029/2008JD009916.

Kalnay, E., and M. Cai, 2003: Impact of urbanization and land-use change on climate. *Nature*, **423**, 528–531, https://doi.org/10.1038/nature01675.

Klink, K., 1999: Trends in mean monthly maximum and minimum surface wind speeds in the coterminous United States, 1961 to 1990. *Climate Res.*, **13**, 193–205, https://doi.org/10.3354/cr013193.

Li, Z., Z. W. Yan, K. Tu, W. D. Liu, and Y. C. Wang, 2011: Changes in wind speed and extremes in Beijing during 1960–2008 based on homogenized observations. *Adv. Atmos. Sci.*, **28**, 408–420, https://doi.org/10.1007/s00376-010-0018-z.

Lin, C., K. Yang, J. Qin, and R. Fu, 2013: Observed coherent trends of surface and upper-air wind speed over China since 1960. *J. Climate*, **26**, 2891–2903, https://doi.org/10.1175/JCLI-D-12-00093.1.

Mao, J., and Coauthors, 2016: Human-induced greening of the northern extratropical land surface. *Nat. Climate Change*, **6**, 959–964, https://doi.org/10.1038/nclimate3056.

Markowski, P., and Y. Richardson, 2010: *Mesoscale Meteorology in Midlatitudes*. Wiley-Blackwell, 430 pp.

McVicar, T. R., T. G. Van Niel, L. T. Li, M. L. Roderick, D. P. Rayner, L. Ricciardulli, and R. J. Donohue, 2008: Wind speed climatology and trends for Australia, 1975–2006: Capturing the stilling phenomenon and comparison with near-surface reanalysis output. *Geophys. Res. Lett.*, **35**, L20403, https://doi.org/10.1029/2008GL035627.

——, and Coauthors, 2012: Global review and synthesis of trends in observed terrestrial near-surface wind speeds: Implications for evaporation. *J. Hydrol.*, **416–417**, 182–205, https://doi.org/10.1016/j.jhydrol.2011.10.024.

Minola, L., C. Azorin-Molina, and D. Chen, 2016: Homogenization and assessment of observed near-surface wind speed trends across Sweden, 1956–2013. *J. Climate*, **29**, 7397–7415, https://doi.org/10.1175/JCLI-D-15-0636.1.

Myneni, R. B., C. D. Keeling, C. J. Tucker, G. Asrar, and R. R. Nemani, 1997: Increased plant growth in the northern high latitudes from 1981 to 1991. *Nature*, **386**, 698–702, https://doi.org/10.1038/386698a0.

Nonaka, M., and S. P. Xie, 2003: Covariations of sea surface temperature and wind over the Kuroshio and its extension: Evidence for ocean-to-atmosphere feedback. *J. Climate*, **16**, 1404–1413, https://doi.org/10.1175/1520-0442(2003)16<1404:COSSTA>2.0.CO;2.

Ozdogan, M., G. D. Salvucci, and B. T. Anderson, 2006: Examination of the Bouchet–Morton complementary relationship using a mesoscale climate model and observations under a progressive irrigation scenario. *J. Hydrometeor.*, **7**, 235–251, https://doi.org/10.1175/JHM485.1.

Pryor, S. C., and Coauthors, 2009: Wind speed trends over the contiguous United States. *J. Geophys. Res.*, **114**, D14105, https://doi.org/10.1029/2008JD011416.

Raupach, M. R., 1992: Drag and drag partition on rough surfaces. *Bound.-Layer Meteor.*, **60**, 375–395, https://doi.org/10.1007/BF00155203.

——, 1994: Simplified expressions for vegetation roughness length and zero-plane displacement as functions of canopy height and area index. *Bound.-Layer Meteor.*, **71**, 211–216, https://doi.org/10.1007/BF00709229.

Ren, G. Y., Y. Q. Zhou, Z. Y. Chu, J. X. Zhou, A. Y. Zhang, J. Guo, and X. F. Liu, 2008: Urbanization effects on observed surface air temperature trends in north China. *J. Climate*, **21**, 1333–1348, https://doi.org/10.1175/2007JCLI1348.1.

Roderick, M. L., L. D. Rotstayn, G. D. Farquhar, and M. T. Hobbins, 2007: On the attribution of changing pan evaporation. *Geophys. Res. Lett.*, **34**, L17403, https://doi.org/10.1029/2007GL031166.

Schlatter, T. W., G. W. Branstator, and L. G. Thiel, 1976: Testing a global multivariate statistical objective analysis scheme with observed data. *Mon. Wea. Rev.*, **104**, 765–783, https://doi.org/10.1175/1520-0493(1976)104<0765:TAGMSO>2.0.CO;2.

Si, P., C. Luo, and D. Liang, 2018: Homogenization of Tianjin monthly near-surface wind speed using RHtestsV4 for 1951–2014. *Theor. Appl. Climatol.*, **132**, 1303–1320, https://doi.org/10.1007/s00704-017-2140-7.

Sun, Y., X. B. Zhang, G. Y. Ren, F. W. Zwiers, and T. Hu, 2016: Contribution of urbanization to warming in China. *Nat. Climate Change*, **6**, 706–710, https://doi.org/10.1038/nclimate2956.

Troccoli, A., K. Muller, P. Coppin, R. Davy, C. Russell, and A. L. Hirsch, 2012: Long-term wind speed trends over Australia. *J. Climate*, **25**, 170–183, https://doi.org/10.1175/2011JCLI4198.1.

Vautard, R., J. Cattiaux, P. Yiou, J.-N. Thépaut, and P. Ciais, 2010: Northern Hemisphere atmospheric stilling partly attributed to an increase in surface roughness. *Nat. Geosci.*, **3**, 756–761, https://doi.org/10.1038/ngeo979.

Wan, H., X. L. Wang, and V. R. Swail, 2010: Homogenization and trend analysis of Canadian near-surface wind speeds. *J. Climate*, **23**, 1209–1225, https://doi.org/10.1175/2009JCLI3200.1.

Wang, K., R. E. Dickinson, and S. Liang, 2009: Clear sky visibility has decreased over land globally from 1973 to 2007. *Science*, **323**, 1468–1470, https://doi.org/10.1126/science.1167549.

——, Q. Ma, Z. Li, and J. Wang, 2015: Decadal variability of surface incident solar radiation over China: Observations, satellite retrievals, and reanalyses. *J. Geophys. Res.*, **120**, 6500–6514, https://doi.org/10.1002/2015JD023420.

Wang, X. L., 2008: Penalized maximal F test for detecting undocumented mean shift without trend change. *J. Atmos. Oceanic Technol.*, **25**, 368–384, https://doi.org/10.1175/2007JTECHA982.1.

——, F. W. Zwiers, V. R. Swail, and Y. Feng, 2009: Trends and variability of storminess in the northeast Atlantic region, 1874–2007. *Climate Dyn.*, **33**, 1179–1195, https://doi.org/10.1007/s00382-008-0504-5.

Wever, N., 2012: Quantifying trends in surface roughness and the effect on surface wind speed observations. *J. Geophys. Res.*, **117**, D11104, https://doi.org/10.1029/2011JD017118.

Wong, M. S., and J. E. Nichol, 2012: Spatial variability of frontal area index and its relationship with urban heat island intensity. *Int. J. Remote Sens.*, **34**, 885–896, https://doi.org/10.1080/01431161.2012.714509.

Wu, J., J. Zha, and D. Zhao, 2016: Estimating the impact of the changes in land use and cover on the surface wind speed over the East China Plain during the period 1980–2011. *Climate Dyn.*, **46**, 847–863, https://doi.org/10.1007/s00382-015-2616-z.

——, ——, ——, and Q. Yang, 2018a: Changes in terrestrial near-surface wind speed and their possible causes: An overview. *Climate Dyn.*, **51**, 2039–2078, https://doi.org/10.1007/s00382-017-3997-y.

——, ——, ——, and ——, 2018b: Effects of surface friction and turbulent mixing on long-term changes in the near-surface wind speed over the Eastern China Plain from 1981 to 2010. *Climate Dyn.*, **51**, 2285–2299, https://doi.org/10.1007/s00382-017-4012-3.

Xiao, Z., S. Liang, J. Wang, P. Chen, X. Yin, L. Zhang, and J. Song, 2014: Use of general regression neural networks for generating the GLASS leaf area index product from time-series MODIS surface reflectance. *IEEE Trans. Geosci. Remote Sens.*, **52**, 209–223, https://doi.org/10.1109/TGRS.2013.2237780.

——, ——, ——, Y. Xiang, X. Zhao, and J. Song, 2016: Long-time-series global land surface satellite leaf area index product derived from MODIS and AVHRR surface reflectance. *IEEE Trans. Geosci. Remote Sens.*, **54**, 5301–5318, https://doi.org/10.1109/TGRS.2016.2560522.

Xu, C.-Y., L. Gong, T. Jiang, D. Chen, and V. P. Singh, 2006: Analysis of spatial distribution and temporal trend of reference evapotranspiration and pan evaporation in Changjiang (Yangtze River) catchment. *J. Hydrol.*, **327**, 81–93, https://doi.org/10.1016/j.jhydrol.2005.11.029.

Xu, M., C.-P. Chang, C. Fu, Y. Qi, A. Robock, D. Robinson, and H.-M. Zhang, 2006: Steady decline of east Asian monsoon winds, 1969–2000: Evidence from direct ground measurements of wind speed. *J. Geophys. Res.*, **111**, D24111, https://doi.org/10.1029/2006JD007337.

Zeng, X.-M., M. Wang, N. Wang, X. Yi, C. Chen, Z. Zhou, G. Wang, and Y. Zheng, 2018: Assessing simulated summer 10-m wind speed over China: Influencing processes and sensitivities to land surface schemes. *Climate Dyn.*, **50**, 4189–4209, https://doi.org/10.1007/s00382-017-3868-6.

Zhou, C., and K. Wang, 2017: Contrasting daytime and nighttime precipitation variability between observations and eight reanalysis products from 1979 to 2014 in China. *J. Climate*, **30**, 6443–6464, https://doi.org/10.1175/JCLI-D-16-0702.1.

——, ——, and Q. Ma, 2017: Evaluation of eight current reanalyses in simulating land surface temperature from 1979 to 2003 in China. *J. Climate*, **30**, 7379–7398, https://doi.org/10.1175/JCLI-D-16-0903.1.

Zhou, L. M., R. E. Dickinson, Y. Tian, J. Fang, Q. Li, R. K. Kaufmann, C. J. Tucker, and R. B. Myneni, 2004: Evidence for a significant urbanization effect on climate in China. *Proc. Natl. Acad. Sci. USA*, **101**, 9540–9544, https://doi.org/10.1073/pnas.0400357101.

Zhu, Z., and Coauthors, 2016: Greening of the Earth and its drivers. *Nat. Climate Change*, **6**, 791–796, https://doi.org/10.1038/nclimate3004.